Thermal conductivity in a chain of alternately free and bound particles

D. J. R. Mimnagh and L. E. Ballentine
Physics Department, Simon Fraser University, Burnaby, British Columbia, Canada V5A 1S6
(Received 23 June 1997)

The thermal conductivity κ of a lattice of alternately free and harmonically bound particles placed between two temperature reservoirs is calculated for various chain lengths and dimensionless energy ε. It is found that Fourier's law is obeyed for all ε as long as the lattice is long enough. However, this length scale undergoes a transition from essentially an ε independence for $\varepsilon<\varepsilon_c$ to a power-law dependence for $\varepsilon>\varepsilon_c$, meaning that larger lattices are needed to get normal thermal conductivity for large ε. This transition is seen to coincide with a change in scaling law for the maximum Lyapunov exponent λ. This behavior of λ is known to correspond to a transition to total chaos, where all stable regions of phase space have vanished. It is surmised that this measure of the dynamics can be used as a probe of the Fourier law properties of other systems. [S1063-651X(97)11011-X]

PACS number(s): 05.45.+b, 05.60.+w, 66.10.Cb

I. INTRODUCTION

Although Fourier's law of heat conduction (heat current being proportional to the thermal gradient) is very commonly observed, it is far from clear what properties of the dynamical system are responsible for the observed behavior. ''Neither phenomenological nor fundamental transport theory can predict whether or not a given classical many-body Hamiltonian system yields an energy transport governed by the Fourier heat law.'' So reads the first sentence of the paper by Casati, Ford, Vivaldi, and Visscher [1] (CFVV), in which they introduced the so-called ''ding-a-ling'' model, as the simplest system in which the Fourier heat conduction law could be demonstrated. The model consists of a one-dimensional chain of atoms, alternately free and harmonically bound, which interact through hard elastic collisions. CFVV demonstrated that this model exhibits chaotic dynamics and presented numerical evidence that, for moderately long chains, the thermal conductivity approaches a value independent of the length of the chain.

The numerical study of the relation between dynamics and nonequilibrium statistical mechanics began with the work of Fermi, Pasta, and Ulam (FPU), lucidly reviewed by Ford [2]. FPU studied a harmonic chain with weak nonlinearity. Instead of the expected equipartition of energy among the modes, they found a recurrent behavior, which is now known to be related to the Kolmogorov-Arnold-Moser (KAM) theorem, but which was originally very puzzling. Because of the difficulties found by FPU and others, many people came to believe that normal thermal conductivity could not occur in one dimension [3]. However, Mokross and Büttner [4] gave evidence that the diatomic Toda lattice exhibited a transition to normal thermal conductivity, which later was verified by the more detailed numerical investigation of Jackson and Mistriotis [5]. The most persuasive work, however, was that of CFVV who gave arguments for a direct connection between normal thermal conductivity and dynamical chaos in a very simple system. They also showed that the value of the thermal conductivity given by the Green-Kubo formula is in agreement with that obtained directly from numerical simulation.

The original purpose of this work was to examine in more detail the relations between thermal conductivity and aspects of the dynamics, such as Lyapunov exponents. After reproducing the results of CFVV, and extending them, we were surprised to discover that the conductivity value that they had reported as the long-chain limit was actually only a transitory plateau. The thermal conductivity does indeed converge to a long-chain limit, but only at lengths considerably greater than those reported by CFVV. Moreover, the approach to the long-chain limit can be nonmonotonic as a function of length.

The ding-a-ling model is introduced in Sec. II of this paper. In Sec. III we present results for the thermal conductivity, which confirm the earlier results of CFVV, as far as they went, but also show surprising results in regions that they did not explore. We treat the dependence of the conductivity on the spring stiffness, temperature, and chain length in considerable detail. In Sec. III we study the dynamics of the model, illustrating the transition between the weak-spring and stiff-spring limits in several different ways. Finally, we summarize the conclusions.

II. THE DING-A-LING MODEL

The ding-a-ling lattice consists of a set of alternately free and bound particles. The Hamiltonian for the N-particle ding-a-ling model, as described by CFVV, is

$$H=\frac{1}{2}\sum_{i=1}^{N}(v_i^2+\omega_i^2 x_i^2)+(\text{hard point core}), \tag{1}$$

where ω_i equals ω for even i and zero for odd i and all particles have unit mass. Two versions of this model will be studied. To calculate the thermal conductivity, we use an open system, a chain with a free particle at each end, which interacts with a thermal reservoir. To calculate the Lyapunov exponent, we use a closed ring of particles. The open chains contain an odd number of particles and the closed rings contain an even number of particles.

The dynamics of a closed ring depends on only a single dimensionless parameter $\varepsilon=E/\omega^2 l_0^2$, where E is the average

energy per particle and l_0 is the lattice spacing. CFVV fix E and l_0 and use ω as a variable parameter. We use ε as our fundamental parameter and have confirmed the scaling by varying both E and ω in some of our calculations.

In the case of the chain interacting with reservoirs, the total energy is not fixed, so we must infer its average value from the temperature. The average temperature T_m is midway between the temperature of the left and right reservoirs T_L and T_R. If we assume equipartition then the average energy of the free particles is $\frac{1}{2}T_m$, and the average energy of the bound particles is T_m. This leads to an average energy of a system particle of $\frac{3}{4}T_m$. So the quantity

$$\varepsilon = \frac{3T_m}{4\omega^2} \tag{2}$$

is used to parametrize our open system (we set $l_0=1$ and Boltzmann's constant $k_B=1$).

The parameter ε should be regarded as a conventional reparametrization of the temperature as a dimensionless energy. It is only approximately equal to the energy density (more precisely, the dimensionless energy per particle). The average energy of a free particle is $\frac{1}{2}T$. The average energy of a bound particle ranges from T in the low-density limit to $\frac{1}{2}T$ in the high-density limit, where collisions prevent the spring from stretching very far. As a result, the true energy density ranges from ε to $\frac{2}{3}\varepsilon$ as we go from the low- to the high-density limits. No confusion will arise provided we regard the values of ε for an open chain as merely reexpressing the temperature in dimensionless units. Only when a result computed at constant E is compared with one computed at constant T can any ambiguity of interpretation arise. This is done in Fig. 16, where it does not cause any trouble.

Between collisions the motion has an analytic solution, so in order to evolve it forward in time one must simply calculate the time of the collision events and then evolve the system from collision to collision. This means that the system is more naturally described in terms of a mapping than as a solution to a Hamiltonian with infinite potentials to represent the hard collisions. However, since many of the physical quantities are calculated per unit time, rather than per collision, it is necessary to have a mixed notation. A superscript 0 will identify quantities measured just after the collision and this quantity will have a j subscript to identify which collision. For instance, x_{ij}^0 and v_{ij}^0 represent the position relative to its lattice site and velocity for particle i at the time just after collision j, while $x_i(t)$ and $v_i(t)$ represent the same quantities at the arbitrary time t, measured relative to the first collision. The evolution of the position of particle i between collision j and $j+1$ is

$$x_i(t) = \begin{cases} A_{ij}^0 \sin[\omega(t-\tau_j)+\phi_{ij}^0], & i \text{ even} \\ v_{ij}^0(t-\tau_j)+x_{ij}^0, & i \text{ odd} \end{cases} \tag{3}$$

for $\tau_j < t \leq \tau_{j+1}$, where A_{ij}^0 and ϕ_{ij}^0 are the amplitude and phase of the oscillator and τ_j is the time of the collision j. In order to calculate the time of collision j we must find the possible collision time t_{ij}^0 for each particle pair i and $i+1$ such that

$$x_i(t_{ij}^0) - x_{i+1}(t_{ij}^0) = 1, \tag{4}$$

the term 1 being the lattice spacing. Then we select the soonest collision time as the actual collision time for the system. To complete the collision we must evolve the system to time τ_j and then exchange the velocities of the particles involved in the collision. If we define the systems state (made up of all its position and velocity coordinates) after collision j by Γ_j^0, then

$$\Gamma_j^0 = f(\Gamma_{j-1}^0) \tag{5}$$

maps the physical system from the time of system collision $j-1$ to system collision j and swaps the velocities of the pair of particles involved in the collision.

III. CALCULATION OF THE THERMAL CONDUCTIVITY

A. Method of calculation

The calculation of the thermal conductivity for the system is performed in a manner similar to that described by CFVV [1]. A temperature gradient ∇T is placed across the lattice and the energy flux J is then monitored. The thermal conductivity k is $-J/\nabla T$. To establish the temperature gradient, heat reservoirs at different temperatures are placed at either end of the lattice. These are random number generators that take the particles that enter the reservoir and eject them back into the system with a velocity of the appropriate distribution. The probability distribution used is $P(v)=(|v|/T)\exp(-v^2/2T)$, which is the velocity distribution for particles ejected from a pin hole in the side of an oven. The difference between the energy of the particles entering and leaving during the mth reservoir interaction ΔE_m is used in the calculation of the flux

$$J_n = \frac{1}{t_n}\sum_{m=1}^{n} \Delta E_m \tag{6}$$

after n reservoir interactions. After eliminating the initial transients, a sufficient number of collisions are calculated such that $J_n \approx J_\infty$. The value of the local temperature is calculated as twice the kinetic energy of each particle. Then we assume that the position of the particles is, on average, at its lattice site and perform a linear fit to the data. The slope is the effective temperature gradient ∇T_{eff}. It will, in general, be different from the applied temperature gradient ∇T_{app} because there is a temperature jump at the ends of the lattice, similar to a Kapitza resistance. They function merely as the interface between the reservoir and the system. For this reason the end particles are never included in any of our ∇T_{eff} calculations.

To compare the results for different parameter values, it is useful to consider dimensionless quantities. For example, J/ω^3 is a dimensionless flux and $\kappa \equiv k/\omega$ is a dimensionless thermal conductivity. We have found, as expected, that we obtain approximately the same κ for different T_m and ω if they are chosen such that ε is constant.

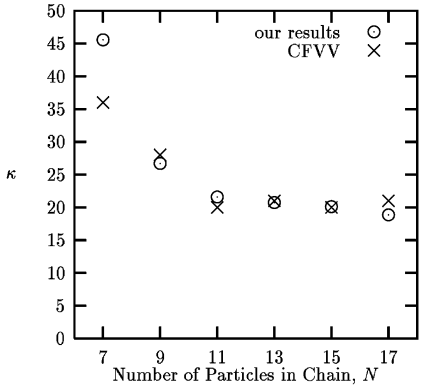

FIG. 1. Comparison of dimensionless thermal conductivity κ with the CFVV results for $\omega=1$ ($\varepsilon=1.5$).

B. Comparison with CFVV

CFVV presented results for the thermal conductivity as a function of the chain length (their Fig. 3). We compared data from their plot with our own data for the equivalent value of ε and with the temperature of the left reservoir T_L set to 2.5 and the right T_R set to 1.5. Our data (Fig. 1), clearly agree with the results of CFVV. However, it is premature to conclude, as CFVV did, that this corresponds to the asymptotic limit of the thermal conductivity. In Fig. 2 we show that this is only a minimum and that bulk thermal conductivity cannot be said to have been observed until $N>200$. The minimum is deepest for large energy densities and disappears entirely for very small density, as can be seen in Fig. 3.

CFVV also produced a table of k, J, and ∇T values for $\omega=10$. These values were also confirmed by our calculations.

C. Temperature dependence of k

If Fourier's law $J=-k\nabla T$ is valid, we would expect that, after initial transients have died out, there would be a uniform gradient of temperature along the chain. Figure 4 shows that the local temperature (computed as twice the average kinetic energy of each particle) actually has a smooth nonlinear variation with position. We interpret the curvature as being due to the temperature dependence of the conductivity k. If k increases with T, then the decrease of $k(T)$ from left to right along the chain must be compensated by an increase in the magnitude of ∇T.

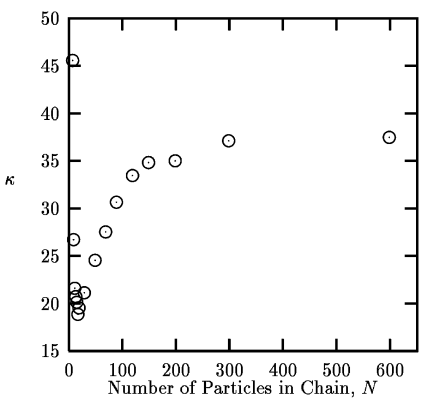

FIG. 2. Thermal conductivity κ for $\omega=1$ ($\varepsilon=1.5$) with very large lattices.

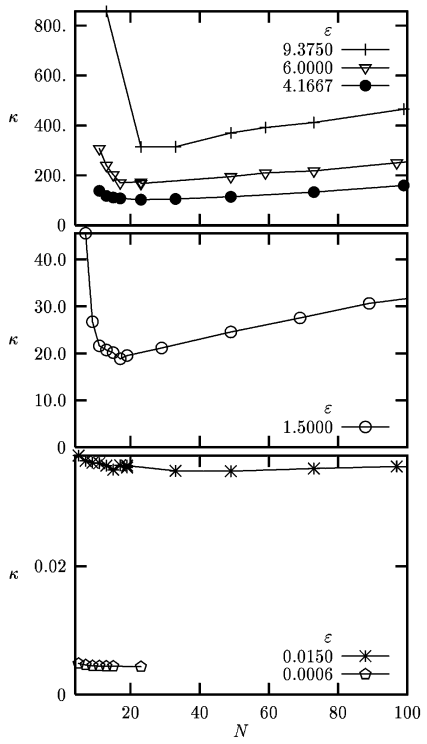

FIG. 3. Thermal conductivity for various numbers of particles N.

We have calculated $k(T)$ directly by varying the central temperature (Fig. 5). To ensure that the variation of $k(T)$ along the chain does not affect our results, we use a small temperature difference ΔT. In Fig. 5 we see results for chains of 9 and 31 particles with $\Delta T=0.2$. The results are different from what one might expect for an anharmonic lattice. For example, the work of Maeda and Munakata [6] shows a different relationship for small T, $k(T)\propto T^{-1/2}$. This is because they were modeling FPU's β lattice (harmonic lattice with quartic anharmonicity). For small T, the anharmonic term will not contribute and one expects a divergent k for an integrable (harmonic) lattice. For the ding-a-ling lattice, as the energy is reduced the bound particles are more tightly bound to there sites. This attenuates solitonlike energy transport, so one does not expect k to diverge as $T\rightarrow 0$; in fact, we see $k\rightarrow 0$ in Fig. 5. On the other hand, the high-T regime should produce divergent k since, in this limit, the lattice behaves like free particles on a wire (an integrable system).

As pointed out by Nishiguchi and Sakuma [7], the curvature in the temperature profile can be a source of error in the calculation of k. In order to measure its effect we tried reducing the applied temperature difference. This incurred a greatly increased convergence time and was only practical for short lattices. In any case, the computed k did not vary appreciably. For longer chains a better solution was to include only the central 60% of the particles in the calculation of ∇T. This section of the lattice has a much more linear T profile and thus a more accurate value of k could be calculated.

From Fig. 5 we see that the region between $T=1.5$ and 2.5 is approximately linear and we shall use this to predict the curvature of $T(x)$ in Fig. 4. Following a procedure de-

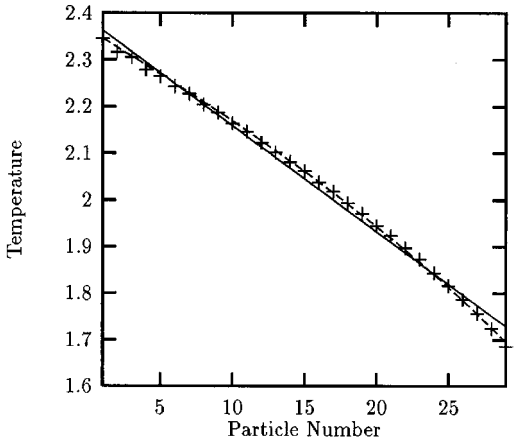

FIG. 4. Temperature profile with $\omega=2$. The solid line is a linear fit through the data and the dashed line is a fit using Eq. (11) with β the only variable parameter.

scribed by Gebhart [8], we approximate $k(T)$ as

$$k(T)=k_r+\beta(T-T_r), \tag{7}$$

where T_r is the temperature of the rightmost ($i=N-1$) particle used in the calculation of k and k_r is $k(T_r)$. From Fourier's law we have

$$\int_{T_l}^{T} k(T')dT' = -\int_{2}^{x} J\,dx', \tag{8}$$

where the leftmost ($i=2$) particle involved has a temperature T_l. Since J is constant along the lattice, we have

$$-\int_{2}^{x} J\,dx' = -J(x-2) \tag{9}$$

and using Eq. (7) we get

$$\int_{T_l}^{T} k(T')dT' = \left[k_rT' + \beta\left(\frac{T'^2}{2} - T_rT'\right)\right]\Bigg|_{T_l}^{T}. \tag{10}$$

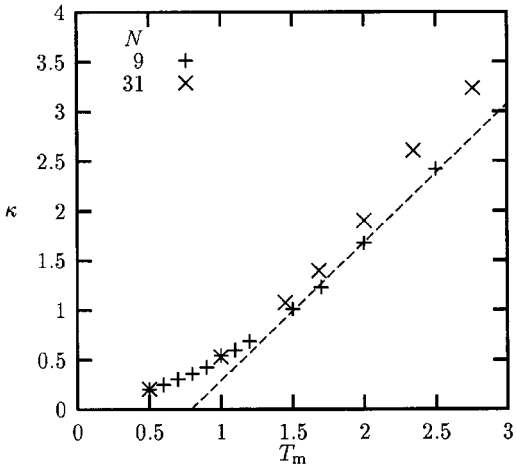

FIG. 5. Value of κ as a function of T, for $\omega=2$ and chain lengths of 9 and 31 particles with $\Delta T=0.2$. The dashed line is a linear fit through the points between 1.5 and 2.5 for $N=9$.

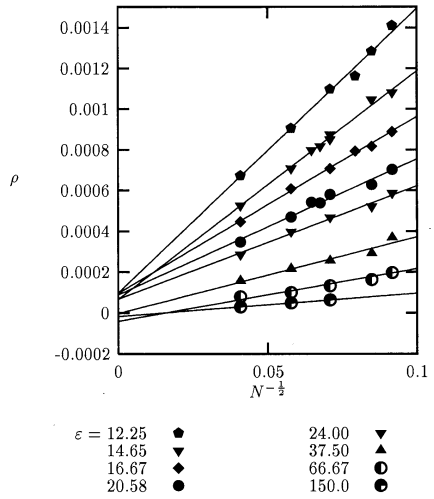

FIG. 6. Resistivity for long chains and large ε. The solid line is a least-squares fit for $N^{-1/2}<0.12$.

We now use these two equations to solve for $T(x)$,

$$T(x) = -\gamma \pm \left\{\gamma^2 - 2\left[\frac{J}{\beta}(x-2) - \frac{k_rT_l}{\beta} - \left(\frac{T_l^2}{2} - T_rT_l\right)\right]\right\}^{1/2}, \tag{11}$$

where γ is $k_r/\beta-T_r$. Notice that the fit for T is exact for $x=2$ (the left end), while k is exact for $T=T_r$ (the right end).

The temperature profile data of Fig. 4 was fitted to formula (11), using β as the only adjustable parameter. The nonlinear least-squares fit yields the value $\beta=3.0$. This may be compared to the slope of the $k(T)$ curve in Fig. 5 at the central temperature $T_m=2$, which yields $\beta=2.8$. The agreement between the two independent determinations of β is satisfactory.

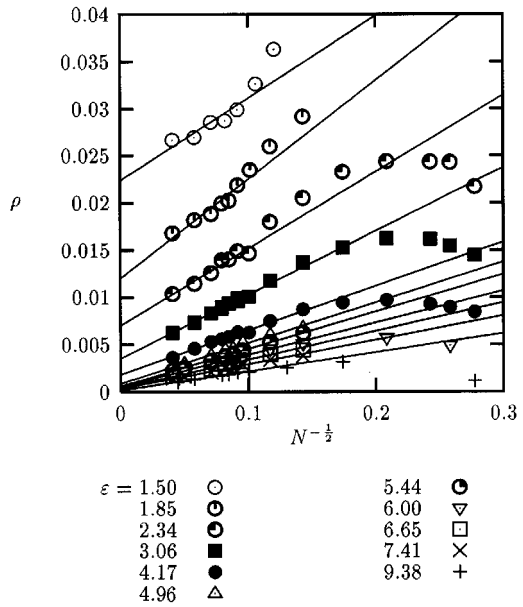

FIG. 7. Resistivity for long chains and medium ε. Only every second data point is displayed for $\varepsilon>4.5$ to make the graph more readable. The solid line is a least-squares fit for $N^{-1/2}<0.12$.

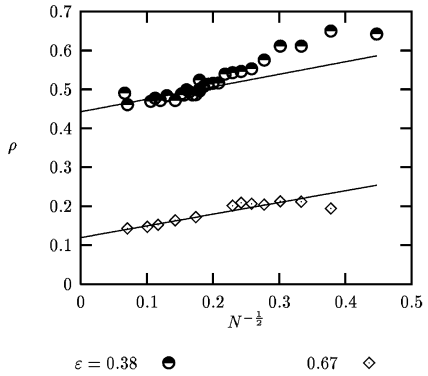

FIG. 8. Resistivity for long chains and small ε. The solid line is a least-squares fit for $N^{-1/2}<0.20$.

D. Long-chain limit

In addition to confirming the results of CFVV, we wish to determine the range of parameters ε and N over which Fourier's law applies. Although Fig. 2 shows clearly that a constant value of κ has been reached in this case, it is more effective to plot the thermal resistivity $\rho=1/\kappa$ as a function of $N^{-1/2}$. We use $N^{-1/2}$ rather than $1/N$ as the variable because it yields a good linear fit for large N (see Figs. 6–9). So the linear function

$$\rho(N)=\mu N^{-1/2}+\rho_\infty \tag{12}$$

is used to describe our large N resistivity data. A positive intercept of the ρ axis ($\rho_\infty>0$) for $N^{-1/2}\to 0$ implies that the conductivity has a finite limit for arbitrarily long chains. A zero intercept implies that κ diverges as $N\to\infty$ and so Fourier's law would not apply. A negative intercept would imply that κ diverges for some finite N. In fact, however, the appearance of a negative intercept in Fig. 6 merely means that the data are insufficient to resolve an intercept very close to zero.

The plots of resistivity (Figs. 6–9) give a fairly complete picture of the behavior as we vary ε. Figure 6 shows the weak-spring limit, in which we might expect Fourier's law to break down. These data demonstrate the limit of our numerical capabilities, since we would need to calculate κ for much longer lattices in order to resolve whether the intercept is

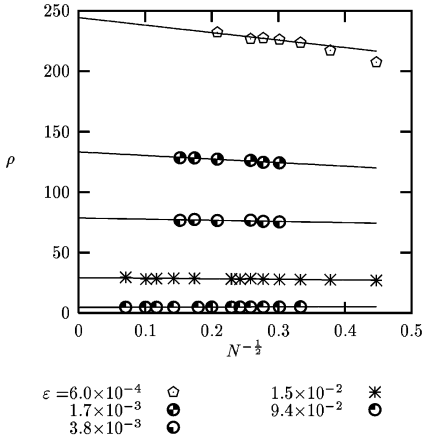

FIG. 9. Resistivity for long chains and very small ε. The solid line is a least-squares fit for $N^{-1/2}<0.32$.

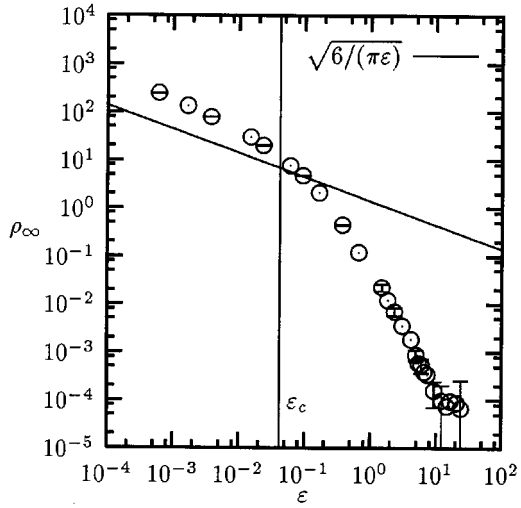

FIG. 10. Resistivity for infinite chains (the intercept in Figs. 7–9). The solid line is a least-squares fit for $1<\varepsilon<10$. The dashed line is the analytic result from Eq. (24).

positive or negative. In Figs. 7 and 8 we can say with confidence that, for these values of ε, we have a positive intercept. We can also see a very distinct maximum in ρ, for some values of ε, which corresponds to the minima in Fig. 3. The maxima have disappeared in Fig. 9.

The intercepts in Figs. 6–9 tell us how the conductivity behaves for an infinite lattice, so it is useful to plot it as a function of ε, as in Fig. 10. (We have not included the intercepts from Fig. 6 since they are not accurate enough.) We can see quite clearly the change in behavior from small ε (stiff springs) to large ε (weak springs). The power-law variation in ρ_∞ for $\varepsilon>\varepsilon_c$ implies that infinite conductivity should occur only in the limit of vanishing spring constant, which is the integrable limit of the free-particle hard point gas. We introduce $\varepsilon_c=0.04$ at this point since it functions well as a benchmark for the breakdown of the stiff-spring limit. Its value is derived from the scaling properties of the

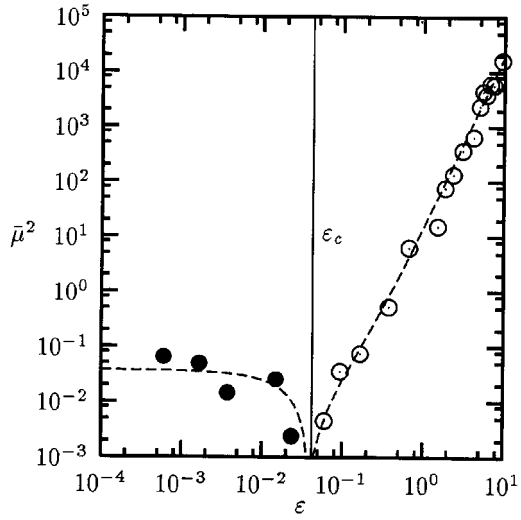

FIG. 11. Square of the normalized slope in Eq. (24). The open circles correspond to a positive slope while the filled circles correspond to a negative slope. The dashed line is used only to guide the eye.

Lyapunov exponent and is discussed fully in Sec. IV E. We will put a vertical bar in our plot at ε_c to distinguish the two regimes: stiff and weak springs.

The slope μ changes sign, with $\mu \lessgtr 0$ for $\varepsilon \lessgtr \varepsilon_c$. If we rewrite Eq. (12) in a normalized form

$$\bar{\rho}(N) = \bar{\mu} N^{-1/2} + 1, \tag{13}$$

where $\bar{\rho} = \rho/\rho_\infty$ and $\bar{\mu} = \mu/\rho_\infty$, then for $\bar{\rho}(N)$ to be within some δ of 1 we must take $N > N_\delta$,

$$N_\delta = \left(\frac{\bar{\mu}}{\delta} \right)^2. \tag{14}$$

Figure 11 shows that as ε increases, for $\varepsilon > \varepsilon_c$, we need increasingly larger lattices to approximate the asymptotic limit; however, for $\varepsilon < \varepsilon_c$ only short lattices are needed and N_δ is not strongly dependent on ε. A dashed line is used in Fig. 11 to emphasize that the slope does go through zero and show the dominant features. Fourier's law is always obeyed provided the lattices are long enough.

E. Stiff-spring limit

It is possible to deduce the value of the thermal conductivity by means of a simple argument, which should be valid in the limit of very stiff springs on the bound particles. We assume that each bound particle behaves as a harmonic oscillator with a Maxwellian velocity distribution governed by the local temperature. A free particle bounces back and forth between two bound particles. At each elastic collision it exchanges velocities with the bound particle and so on average it carries energy from the higher- to the lower-temperature side.

Let v_+ be the speed of a free particle traveling in the positive direction (down the temperature gradient) and v_- be its speed of return in the negative direction. The contribution to the energy flux from this round-trip will be equal to the difference between the energies carried in the two directions, divided by the time for the round-trip,

$$J = \frac{\frac{1}{2} v_+^2 - \frac{1}{2} v_-^2}{\frac{2}{v_+} + \frac{2}{v_-}}. \tag{15}$$

The factor of 2 in the denominator comes from the distance between the bound particles, which is two lattice units.

We can estimate the conductivity if we replace the velocities in Eq. (15) by their rms averages $\bar{v}$, which are related to the temperature by equipartition, $\frac{1}{2}\bar{v}^2 = \frac{1}{2}T$ (Boltzmann's constant has been set to unity). Writing the temperature of the left and right bound particles as $T_+ = T - \nabla T$ and $T_- = T + \nabla T$ and neglecting the difference between v_+ and v_- in the denominator, we obtain $J = -\nabla T/2T^{-1/2}$, whence the conductivity becomes

$$k = -\frac{J}{\nabla T} = \sqrt{\frac{T}{2}}. \tag{16}$$

In terms of our dimensionless parameters $\kappa = k/\omega$ and $\varepsilon = 3T/4\omega^2$, this becomes

$$\kappa = \sqrt{\frac{2}{3}\varepsilon}. \tag{17}$$

A better approximation is obtained if we average the energy current J in Eq. (15) over the distributions of v_+ and v_-. The appropriate distribution $P_T(v)$ is the probability that a free particle will transit at speed v between two bound particles. The Boltzmann distribution, which is the probability that a randomly selected particle will have instantaneous velocity v, differs from $P_T(v)$ by a factor proportional to the transit time (v^{-1}). Hence the appropriate distribution is

$$P_T(v) = \frac{|v|}{T} e^{(-v^2/2T)}. \tag{18}$$

Upon simplifying Eq. (15), we obtain the average energy current

$$\langle J \rangle = \frac{1}{4}[\langle v_+^2 \rangle \langle v_- \rangle - \langle v_+ \rangle \langle v_-^2 \rangle], \tag{19}$$

where the distributions for v_+ and v_- are given by Eq. (18) with temperatures T_+ and T_-, respectively. The calculation of the averages in Eq. (19) are

$$\langle v^2 \rangle = 2T, \tag{20}$$

$$\langle v \rangle = \sqrt{\frac{\pi T}{2}}, \tag{21}$$

so we have

$$J = \sqrt{\frac{\pi}{8}}[T_+ T_-^{1/2} - T_+^{1/2} T_-]. \tag{22}$$

If we now expand J in a Taylor series in ∇T, we have

$$J = -\sqrt{\frac{\pi T}{8}} \nabla T; \tag{23}$$

this results in an approximate value for the conductivity of $k = \sqrt{\pi T/8}$ or in dimensionless variables

$$\kappa = \sqrt{\frac{\pi}{6}\varepsilon}. \tag{24}$$

These are compared with the results of the numerical simulations in Fig. 10, where one can see approximate agreement with the slope corresponding to the exponent of $\frac{1}{2}$ in Eq. (24).

The essential assumption in this simple argument is the neglect of correlations among the particles. This assumption becomes more reasonable in the stiff limit, when the bound particles oscillate very rapidly compared to the motion of the free particles. But the systematic difference between Eq. (24) and the numerical results in Fig. 10 indicates that correlation effects are not entirely negligible, even in that limit.

IV. ANALYSIS OF THE DYNAMICS

In order to demonstrate the role of chaos in establishing Fourier's law of heat conduction, we need to study a system that has both an integrable and a nonintegrable limit. The

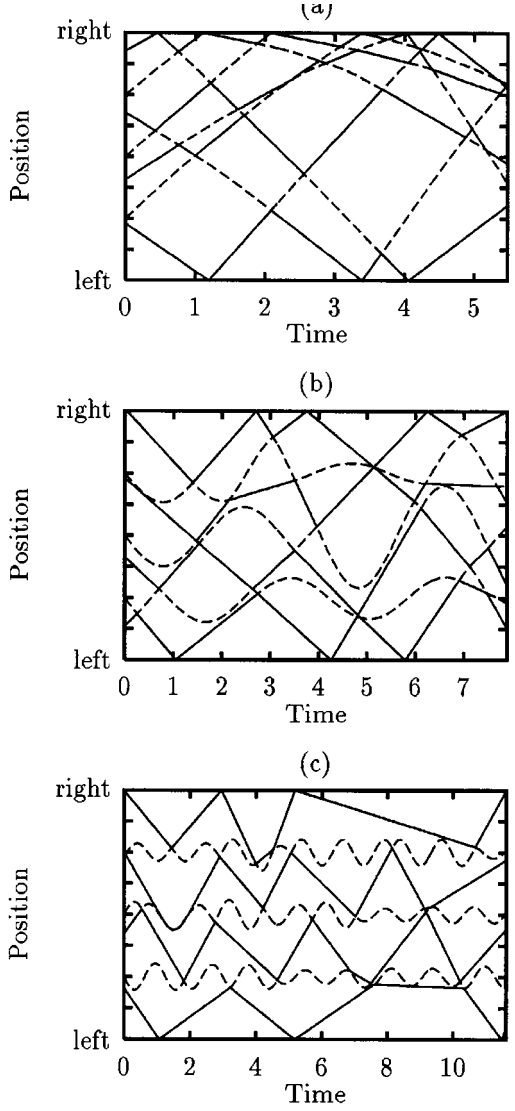

FIG. 12. Lattice dynamics for a seven-particle chain with different ω: (a) $\omega=0.5$ ($\varepsilon=6.0$), (b) $\omega=2$ ($\varepsilon=0.375$), and (c) $\omega=5$ ($\varepsilon=0.06$). The solid lines represent the paths of the free particles, while the dashed lines represent the bound particles.

ding-a-ling model becomes integrable in the zero spring-constant limit. As the spring stiffness increases, the dynamics becomes more chaotic. We wish to observe the transition between two such regimes and to correlate the dynamics with the behavior of the thermal conductivity. The transition between the two regimes is continuous, rather than sharp, but evidence for it can be found in many different aspects of the dynamics.

A. Particle paths

The ding-a-ling model was expected to support a Fourier law conductivity because the energy transport via solitonlike pulses should be suppressed by the phase randomization caused by the oscillating bound particles. In Fig. 12 we see the displacement of particles as a function of time, with the ''left'' and the ''right'' labels on the y axis marking the position of the corresponding reservoirs and the ticks marking the lattice sites.

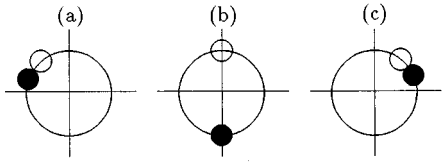

FIG. 13. Two particles on a periodic ring. The solid circle represents a bound particle, while the empty circle represents a free particle.

Particle trajectories cannot cross each other. They merely exchange velocities in elastic collisions. The apparently smooth lines, in Fig. 12(a), from one end of the lattice to the other, represent the transmission of energy without it being scattered or diffused. These solitonlike pulses are typical of the weak-spring limit. As the spring constant increases, the trajectories of the bound particles become more curved, as shown in Fig. 12(b). This causes the solitonlike pulses to propagate along curved paths in the space-time diagram. Sometimes the spatial direction of propagation is reversed, corresponding to the reflection of solitonlike pulses. Energy from the pulse is exchanged with the potential energy of the springs, making solitonlike pulses less effective as a mechanism of energy transport. In the stiff-spring limit [Fig. 12(c)], the pulses are effectively destroyed and diffusive energy transport is dominant. The transition between solitonlike pulses and diffusion being the dominant energy transport mechanism will clearly depend on the length of the lattice. The weaker the spring, the longer the lattice must be in order for energy diffusion to dominate. This is consistent with the results of Figs. 6–9 and 11, which show that as the spring becomes weaker, longer lattices are needed to approximate the bulk conductivity limit.

B. Phase space

Poincaré sections give a strong visual indication of the chaos of the phase space. CFVV present Poincaré sections, for a two-particle system, showing the KAM tori circling a fixed point in the surface of sections. The destruction of this fixed point, with increasing ε, is an indication of the transition between two dynamical regimes.

From the Poincaré section of CFVV, we know that at the fixed point the velocity of the bound particle is equal to the negative of the velocity of the free particle and the section is such that the particles have just collided. The sign of the relative velocities, as defined for the section, is such that the particles would collide on the left of the loop, as in Fig. 13(a). After colliding they exchange velocities and swing around toward the right. By symmetry the particles must both be on their lattice sites at some intermediate time, as in Fig. 13(b). Proceeding to the right, the particles collide again [Fig. 13(c)] and retrace their pathes back to the state described by Fig. 13(a). The fixed point thus maps the system from a configuration similar to that shown in Fig. 13(a) on to itself.

To analytically explain the fixed point's destruction we need to evaluate the position of the fixed point in phase space. Since the particles have just collided, their positions must satisfy Eq. (4),

$$x_b - x_f = 1, \tag{25}$$

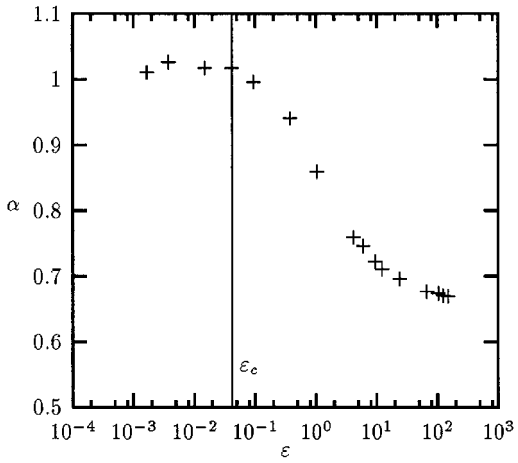

FIG. 14. Ratio of the true energy density to ε for a 99-particle reservoir system.

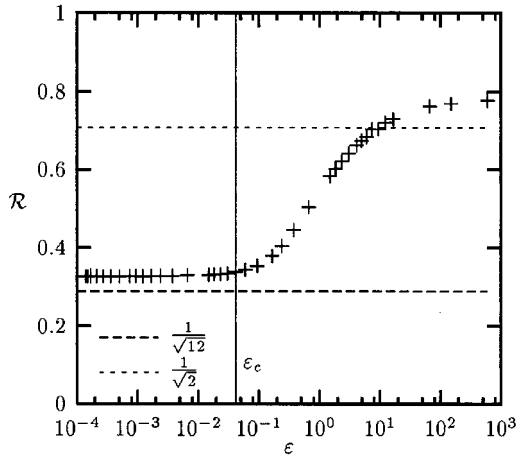

FIG. 15. Reduced collision rate per particle for a 98-particle periodic ring.

where x_f and x_b are the position of the free and bound particles relative to their respective lattice sites. Also, the velocities are equal in size but opposite in direction, so

$$-v_f = v_b = v, \tag{26}$$

where v_f and v_b are the velocities of the free and bound particles after the collision. From energy conservation we have

$$E = \frac{1}{2}v^2 + \frac{1}{2}v^2 + \frac{1}{2}\omega^2 x_b^2 = 2, \tag{27}$$

where we have made use of the initial condition on the energy as specified by CFVV. Solving for v yields

$$v = \left(2 - \frac{1}{2}\omega^2 x_b^2\right)^{1/2}. \tag{28}$$

The time t to travel from (b) to (a) is the same for both particles, hence

$$t = \frac{x_f}{-v} = \frac{1}{\omega}\arctan\frac{\omega x_b}{v}. \tag{29}$$

Using this with Eqs. Eq. (28) and (25) and solving numerically for v, x_f, and x_b we can predict the position of the fixed point in phase space. There are no real solutions for $\varepsilon > 0.151$ (corresponding to $\omega > 2.57$ for an energy per particle of 1 as specified by CFVV), which is consistent with the Poincaré sections. This dimensionless energy $\varepsilon_p = 0.151$ is a convenient marker to identify the values of ε for which we may expect to see changes in the properties of the physical quantities of our system. It will be particularly relevant measurements made to short chains.

C. Energy density

As mentioned in Sec. II, the true energy density is equal to ε in the stiff-spring limit, but is only $\frac{2}{3}$ of ε in the free particle limit. By calculating

$$\alpha = \frac{E/\omega^2}{\varepsilon}, \tag{30}$$

where E is the energy per particle, we will have a measure of which regime we are in for a particular ε. In Fig. 14 we can see that there is a transition region around $\varepsilon = 1$ separating the two limits. The total energy of the system can be attributed to three different sources. In the stiff-spring limit $\frac{1}{3}$ of the total comes from the kinetic energy of the free particles, $\frac{1}{3}$ from the kinetic energy of the bound particles, and $\frac{1}{3}$ from the potential-energy of the bound particles. In the weak-spring limit ($\varepsilon \to \infty$) the potential energy contribution becomes negligible. This leads to $\alpha_\infty = \frac{2}{3}$ in this limit and $\alpha_0 = 1$ in the opposite limit where the potential energy is not restricted.

From Fig. 14 we see the value of α is slightly greater than 1 in the stiff-spring limit, which may be attributed to the temperature dependance of κ. This causes the average temperature of the lattice to be larger than the average of the two reservoirs T_m.

This quantity α plays a role in our calculation when we wish to know the temperature of a periodic chain because in this case we specify the energy via the initial conditions not the temperature. Rewriting Eq. (30) using the definition of ε [Eq. (2)], we have

$$T_m = \frac{4E}{3\alpha}. \tag{31}$$

D. Collision rate

The collision rate also shows a transition region that divides the two asymptotic limits. The definition of the collision rate per particle is

$$R = \frac{1}{2\tau}, \tag{32}$$

where τ is the typical time between collisions and each collision takes place between two particles. In order to determine the asymptotic limits we need to estimate τ.

In the stiff-spring limit of $\varepsilon \to 0$, with a free and a bound particle originally at their respective origins, the position of the collision is determined by the amplitude of the oscillator. That is, since the oscillator's deviation from equilibrium is small, due to the strong spring, we can assume that a typical collision also takes place near the equilibrium position of the oscillator. We can estimate the time between such collisions as the time it takes the free particle to travel from its lattice site to the bound particles lattice site and back. To do this we make use of the collision definition (4),

$$v_f \frac{\tau}{2} - 0 = 1, \tag{33}$$

where v_f is the velocity of the free particle and the time τ includes both the time to travel from the origin to the collision and back. We have chosen particle i to be a free particle and particle $i+1$ to be a bound particle, so v_f is a positive quantity, and from equipartition of energy we have $v_f = \sqrt{T_m}$. This leads to a collision rate of $R_0 = \sqrt{T_m}/4$ in the stiff-spring limit.

We now approximate R_∞, the collision rate in the $\varepsilon \to \infty$ limit. The bound particle behaves like a free particle, $v_f \approx -v_b \approx \sqrt{T_m}$; thus

$$v_f \frac{\tau}{2} - v_b \frac{\tau}{2} = 1 \tag{34}$$

which leads to a value of $R_\infty = \sqrt{T_m}/2$.

We would like to remove the ε dependence present in the limiting values in the form of $\sqrt{T_m}$. Since it is E and not T_m that we specify in the closed system, we define the reduced collision rate $\mathcal{R}$ as

$$\mathcal{R} = \frac{R}{\sqrt{E}} = \frac{R}{\sqrt{\frac{3}{4}\alpha T_m}}, \tag{35}$$

where we made use of Eq. (31). This quantity is calculated for a 98-particle chain in Fig. 15 and shows two distinct limiting values. Using Eq. (35) we have estimates of $\mathcal{R}$ in the two limits

$$\mathcal{R}_0 = \frac{1}{4\sqrt{\frac{3}{4}\alpha_0}} = \frac{1}{\sqrt{12}}, \tag{36}$$

$$\mathcal{R}_\infty = \frac{1}{2\sqrt{\frac{3}{4}\alpha_\infty}} = \frac{1}{\sqrt{2}}, \tag{37}$$

which can be seen to agree well with the asymptotes in Fig. 15. The discrepancies are probably due to the neglected correlations.

E. Lyapunov exponents

The maximum Lyapunov exponent λ is a common indicator of the onset of chaos and would appear to be an ideal candidate for a dynamical indicator of the transition to normal thermal conductivity. We see from the definition of λ,

$$\lambda = \lim_{\substack{\delta\Gamma \to 0 \\ t \to \infty}} \frac{1}{t} \ln\left(\frac{\| \Gamma(\Gamma_0 + \delta\Gamma, t) - \Gamma(\Gamma_0, t) \|}{\| \delta\Gamma \|} \right), \tag{38}$$

that λ is a long-time average measuring the exponential rate of separation of trajectories that are initially close in phase space. So we have $\lambda > 0$ in a chaotic region and $\lambda = 0$ in a stable region. However, the relevant time scales for the conduction of heat via a lattice are the time for a particle to cross a lattice spacing or the transit time of solitonlike pulses across the lattice. These times are short, so the relevance of the long-time average λ on its own is uncertain, but will be made clear in what follows.

1. Calculation of λ

The Lyapunov exponent was calculated on a per collision basis λ_C, which eliminates some technical problems with attempts to calculate the Lyapunov exponent on a per unit time basis λ_t. The definition of λ_C is

$$\lambda_C = \lim_{\substack{\delta\Gamma \to 0 \\ n \to \infty}} \frac{1}{n} \ln\left(\frac{\| \Gamma_n^0(\Gamma_0 + \delta\Gamma) - \Gamma_n^0(\Gamma_0) \|}{\| \delta\Gamma \|} \right), \tag{39}$$

where n is the collision index. The calculation of the Lyapunov exponent for a map is outlined by Rasband [9]. Briefly, one evolves both a fiducial and a perturbed trajectory from just after one collision to just after the next collision. Then one renormalizes the perturbed trajectory with a scale factor. The maximum Lyapunov exponent is simply the sum of the logarithm of these scales divided by the total number of collisions.

The problem with the direct calculation of λ_t results from the fact that the time between collisions for the perturbed and fiducial trajectories will be slightly different. This may make the renormalization step impossible without having the particles pass through one another, which is forbidden. We have estimated λ_t by calculating the product of λ_C and the collision rate. This is an acceptable approximation as long as the difference between the time of collision for the perturbed and fiducial trajectories does not contribute on average.

The numerical computation of λ can be tricky. The computed value may appear to be converging to a limit, only to abruptly shift to another value. This sequence of apparent convergences may depend on the initial conditions, even within a single chaotic region of phase space. Only when the trajectory has sampled all of the available phase space can we be sure of true convergence and that is hard to ensure for a many-particle system. We have verified that our results for λ are not sensitive to changes in the initial conditions, size of the displacement of the perturbed trajectory from the fiducial trajectory, and the type of norm used to measure the separation between trajectories.

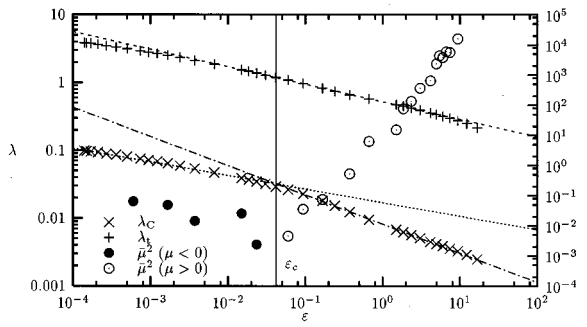

FIG. 16. Lyapunov exponent for 98-particle lattice with λ calculated both per unit time and per collision. For comparison $\bar{\mu}^2$ is replotted.

2. Results for the λ calculation

Like the energy density and the collision rate, the Lyapunov exponent displays a change in behavior during the transition between the two limits. In Fig. 16 we see that λ_C obeys a power law with a sharp change in slope. A power-law fit of the data for the two limits is also shown in Fig. 16 to emphasize the behavior. λ_t also obeys a power law, with some deviations; however, the deviations are less evident. Since the ratio of λ_C and λ_t is the collision rate and the collision rate displays two essentially constant regions separated by a transition region, one would expect to see some reflection of this in Fig. 16. The sharp change in slope for λ_C is at approximately the same ε as the start of the transition region in both Figs. 14 and 15. While there is some evidence of a change of behavior for λ_t at $\varepsilon \approx 10$ (where the transition region ends), more data would be required to confirm this.

The data in Fig. 16 is for a 98-particle lattice from which we infer the behavior of an infinite lattice. To understand how the features in Fig. 16 depend on lattice size, we show some smaller lattices in Fig. 17. As expected, ε_p accurately predicts the transition in the two-particle case, but for 98 particles the transition occurs at a smaller ε. Note also that for $N > 2$ there is a noticeable curvature that changes from convex to concave. This feature is still noticeable for $N = 98$.

An idea by Pettini and Landolfi [10] may explain the physical significance of the change of slope in Fig. 16. They studied the time to equipartion of two different coupled anharmonic oscillator systems and found that there is a change in scaling behavior for $\lambda(\varepsilon)$ beyond the energy density for

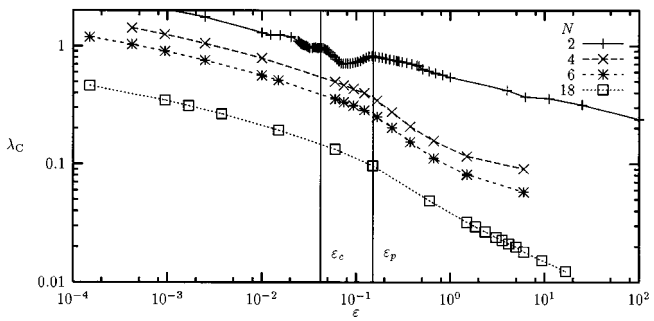

FIG. 17. Lyapunov exponent, calculated per collision, for small lattices.

which all stable regions of phase space disappear. The value of the energy density at which this strong stochasticity threshold, as they call it, occurs was later verified by an analytical technique [11].

In the work of Pettini and Landolfi the time scale for a system's approach to equipartition was studied and two time scales, one fast and one slow, were discovered. The slow approach to equipartition is characteristic of a system soon after the onset of chaos. In this case chaotic trajectories diffuse through phase space along the intersection of the homoclinic manifold of the large-dimensional phase space, that is, along the threads of the so-called Arnold web. As the energy density increased, a transition in the time scale to equipartition was observed. This is due to a breakdown of the Arnold web, so that now the system is able to diffuse freely rather than just along the resonances. This transition in time scales is seen to occur at the same critical dimensionless energy as the strong stochasticity threshold.

We have found very similar results for conductivity in the ding-a-ling system. In Fig. 16 there is a change in the power-law dependence of our Lyapunov exponent calculations at the same dimensionless energy as a change in *length* scale for convergence to a Fourier law conductivity. Pettini and Landolfi found that for $\varepsilon > \varepsilon_c$ the *time* to reach equipartition for a system with only a few initially excited normal modes increased as a power law, while for $\varepsilon < \varepsilon_c$ the *time* was independent of ε. We have seen in Fig. 11 that the *length* scale needed to reach a Fourier law regime had both a power law and an approximately constant region. Note that the integrable limit for the ding-a-ling system is high energy, rather than low energy as in the systems studied by Pettini and Landolfi, so the dependence of the transition on energy density is reversed.

Since the strong stochasticity threshold is meant to indicate the destruction of all stable regions in our large-dimensional phase space, it is instructive to also look at λ for the two-particle case in Fig. 17, since then we have Poincaré sections that will confirm this. There is a lot of structure around $\varepsilon = \varepsilon_p$, which corresponds to the dimensionless energy of the destruction of the main fixed point. The solid vertical line at ε_p does indeed appear to separate different kinds of behavior for the Lyapunov exponent. For larger N the transition ε is smaller, converging to the value ε_c as shown in Fig. 16.

In Fig. 16 we see that the transition in the value of $\bar{\mu}^2$ coincides with the transition in λ. In Ref. [10] it was stressed that equipartition is always reached if one waits long enough and that the transition is simply one of scale. For our system we find that the Fourier law should always be obeyed if one makes the lattice large enough.

V. CONCLUSION

We have shown that, although CFVV were premature in their declaration, the ding-a-ling system does indeed obey Fourier's law. In fact, this Fourier law behavior is very robust, so that the system shows normal thermal conduction for all parameter ranges as long as the lattice is long enough. We have also gained a better understanding of the ding-a-ling model. Its simplicity allowed us to make largely accurate predictions about the shape of the temperature profile, the

scaling of the conductivity in the stiff-spring limit, the destructions of the main fixed point in CFVV's Poincaré sections, and the collision rate in the two limits, the stiff and weak springs.

By extrapolating resistivity to infinite chains, we were able to show that the conductivity should not diverge for any finite dimensionless energy ε. Then using the square of the normalized slope of the resistivity $\bar{\mu}^2$ versus chain length we were able to quantify the length scale for which a normal conductivity was reached. From this we found that for stiff springs the length of chain needed for normal thermal conductivity was insensitive to ε, while for weak springs this N_δ was strongly dependent on ε, obeying a power law. To get a normal thermal conductivity required longer and longer lattices for larger ε. These $\bar{\mu}^2$ data therefore attempt to quantify what is meant by the thermodynamic limit.

A dominant theme running throughout this work is the distinction between the stiff- and weak-spring limits. The reduced collision rate and ratio of the dimensionless and actual energy densities most clearly show the extent of these asymptotic limits and the range of the transition region. In particular, they established that the changes in length scale of the thermal conductivity κ coincide with the onset of this transition.

The graph of the logarithm of the Lyapunov exponent versus the logarithm of ε shows a change in slope at the same value of ε as does the length scale $\bar{\mu}^2$. The importance of this result, in addition to being another dynamical measure that predicts changes in the conductivity of the system, is that it allows us to make contact with a theoretical basis for an understanding of the role of chaos in thermal conductivity. By drawing analogies with the work of Pettini and Landolfi [10], we suggest that there are differences between the thermal conductivity of a dynamical system that is weakly chaotic and one that is totally chaotic. Thermal conductivity across the lattice is enhanced when the trajectories in phase space are allowed to travel across as well as along the resonances.

We found no transition to infinite thermal conductivity, as all our calculations show that Fourier's law will be obeyed for a large enough system. As $\varepsilon \to \infty$ the length of the system that is needed to approximate Fourier's law also diverges to infinity. Since $\varepsilon \to \infty$ is the integrable limit of the free particle gas, it would seem that the transition from finite to infinite thermal conductivity relies on the presence or absence of chaos. Finally, we note that the nonmonotonic approach of the conductivity to its infinite lattice limit, which escaped the notice of CFVV, is an interesting phenomenon whose explanation is not yet fully understood.

ACKNOWLEDGMENT

The authors are grateful for the support provided by the National Science Engineering Research Council of Canada.

[1] G. Casati, J. Ford, F. Vivaldi, and W. M. Visscher, Phys. Rev. Lett. **52**, 1861 (1984).
[2] J. Ford, Phys. Rep. **213**, 271 (1992).
[3] R. A. MacDonald and D. H. Tsai, Phys. Rep. **46**, 1 (1978).
[4] F. Mokross and H. Büttner, J. Phys. C **16**, 4539 (1983).
[5] E. A. Jackson and A. D. Mistriotis, J. Phys. Condens. Matter **1**, 1223 (1989).
[6] A. Maeda and T. Munakata, Phys. Rev. E **52**, 234 (1995).
[7] N. Nishiguchi and T. Sakuma, J. Phys. Condens. Matter **2**, 7575 (1990).
[8] B. Gebhart, *Heat Conduction and Mass Diffusion* (McGraw-Hill, New York, 1993).
[9] S. N. Rasband, *Chaotic Dynamics of Nonlinear Systems* (Wiley, New York, 1990).
[10] M. Pettini and M. Landolfi, Phys. Rev. A **41**, 768 (1990).
[11] L. Casetti, R. Livi, and M. Pettini, Phys. Rev. Lett. **74**, 375 (1995).